Ge$_{1-x}$Sn$_x$ Optical Devices: Growth and Applications

Y. Shimura[a,b,c], W. Wang[a,b], W. Vandervorst[a,b], F. Gencarelli[a,d], A. Gassenq[e,f],
G. Roelkens[e,f], A. Vantomme[b], M. Caymax[a], and R. Loo[a]

[a] Imec, Kapeldreef 75, Leuven, 3001, Belgium [b] Instituut voor Kern- en Stralingsfysica, KU Leuven, 3001 Leuven, Belgium [c] FWO Pegasus Marie Curie Fellow [d] Dept. of Metallurgy and Materials Engineering, KU Leuven, Kasteelpark Arenberg 44, B-3001 Leuven, Belgium [e] Photonics Research Group, INTEC Department, Ghent University-imec, Sint-Pietersnieuwstraat 41, 9000 Ghent, Belgium [f] Center for Nano- and Biophotonics (NB-Photonics), Ghent University, Sint-Pietersnieuwstraat 41, 9000 Belgium

We will introduce our Ge$_{1-x}$Sn$_x$ epitaxial growth process and we will illustrate its material quality by the performance of photodetectors containing a Ge/Ge$_{1-x}$Sn$_x$/Ge quantum well with fully strained Ge$_{1-x}$Sn$_x$ layers. The photodetector responsivity in the short-wave infrared increases with Sn concentration, due to the shrinkage of the band gap. The use of multi quantum wells leads to a higher detector responsivity as the total absorption layer thickness is increased without undesired strain relaxation. The use of Ge$_{1-x}$Sn$_x$ as direct band gap material is expected to boost the efficiency of Ge based photodetectors even further but it requires relaxed Ge$_{1-x}$Sn$_x$ layers. An improvement of the surface quality of the epitaxial Ge$_{1-x}$Sn$_x$ in terms of Sn agglomeration has been achieved by freezing Sn atoms (which is realized by using a high precursor partial pressure and the surfactant effect of hydrogen) into the subsurface of the Ge$_{1-x}$Sn$_x$ layers.

Introduction

Ge$_{1-x}$Sn$_x$, a group IV alloy, is an attractive material for implementation in both electrical and optical devices due to its excellent material properties as described below. Using compressively strained Ge$_{1-x}$Sn$_x$ as a channel, high performance pMOSFETs (Metal-Oxide-Semiconductor field effect transistors) have been reported [1,2]. This is attributed to the hole mobility enhancement due to compressive strain from the Ge substrate. For an nMOSFET, a Ge$_{1-x}$Sn$_x$ buffer layer, which has a larger lattice constant than bulk Ge, can be used as a stressor to create a biaxial tensile strained Ge channel to boost electron mobility [3,4].

On the other hand, Ge$_{1-x}$Sn$_x$ has also gathered attention as a promising candidate as an active material in optical interconnect applications using optical devices such as lasers and photodetectors. The direct band gap of pure Ge corresponds to the favorable wavelength of 1.55 µm for optical communication. In addition, the introduction of Sn (which has a smaller band gap than Ge) into the Ge lattice enables to shrink its band gap. As a result, photodetectors with high responsivity over the complete telecommunication wavelength window by the shift of the absorption spectrum to longer wavelengths can be realized.

The strain state in the $Ge_{1-x}Sn_x$ layers has to be taken into account because the $Ge_{1-x}Sn_x$ active region in the photodetector is grown on a mismatched (Ge on) Si substrate. Both relaxed $Ge_{1-x}Sn_x$ and compressively strained $Ge_{1-x}Sn_x$ have a smaller band gap than pure Ge [5]. On one hand, a fully strained $Ge_{1-x}Sn_x$ layer is favorable to prevent unwanted recombination of electron-hole pairs at dislocations which are generated in case of strain relaxation of the film. On the other, a thick achieve region is required to achieve a higher photodetector responsivity. To achieve the thick active region without the introduction of dislocations, we proposed a $Ge_{1-x}Sn_x$ based strained multi quantum well (QW) photodetector structure [6].

Sn is a direct band gap material. Therefore, for sufficiently high Sn incorporation, $Ge_{1-x}Sn_x$ is predicted to become a direct band gap material [5,7]. Thanks to both the band gap shrinkage by Sn incorporation and the transition to a direct band gap material, a drastic enhancement of the photodetector responsivity is expected. According to our theoretical calculations [5], fully strain relaxed $Ge_{1-x}Sn_x$ becomes a direct band gap material if the substitutional Sn exceeds around 11%. In contrast, when the layer experiences compressive strain, the critical Sn content to achieve the direct transition increases in comparison to the fully strain relaxed case. Therefore, strain relaxation of the $Ge_{1-x}Sn_x$ layer with a sufficiently high (>11%) Sn content is necessary to achieve the transition from indirect to direct band gap material. The required high Sn content exceeds the solubility limit of Sn into Ge. Still, many groups succeeded to develop suitable fabrication schemes for the epitaxial $Ge_{1-x}Sn_x$ growth [8-11]. However, it is still necessary to address layer quality, such as the surface morphology and defects (like dislocations, and Sn precipitations), especially for thick relaxed $Ge_{1-x}Sn_x$ layers.

One obvious option to obtain a highly strain-relaxed epitaxial $Ge_{1-x}Sn_x$ layer with a high Sn content is to increase its thickness. To obtain a sufficiently high degree of relaxation (DSR), the thickness of the $Ge_{1-x}Sn_x$ layer has to be far above the critical thickness for strain relaxation. Even thicker layers are necessary to reduce the threading dislocation density [12]. These layers are expected to be sufficiently thick, as needed in high efficiency optical devices. Sn segregation to the growing surface during epitaxial growth is a well-known problem [13]. It results in Sn agglomerations on the surface when a thick layer is grown. The Sn agglomeration is the result of the collisions among Sn atoms on the surface. Therefore, we focused on the freezing of Sn atoms into the subsurface during $Ge_{1-x}Sn_x$ growth.

In this paper, we first illustrate the material quality of our epitaxial $Ge_{1-x}Sn_x$ layer by the performance of photodetectors containing single and multi $Ge/Ge_{1-x}Sn_x/Ge$ quantum wells with fully strained $Ge_{1-x}Sn_x$ layers. Because, direct band gap material are expected to boost the efficiency of Ge based photodetectors even further, we will also address the surface quality of the epitaxial $Ge_{1-x}Sn_x$ in terms of Sn agglomeration and the impact of the epitaxial growth conditions on this Sn surface agglomeration.

Experimental

$Ge_{1-x}Sn_x$ layers were grown by atmospheric pressure CVD in a 200 mm Epsilon-like equipment from ASM [9]. Before $Ge_{1-x}Sn_x$ growth, the Ge substrates or Ge buffered Si substrates received an *ex-situ* HF (2%) wet etch and an *in-situ* bake in H_2 at 650ºC and

5.3×10^3 Pa in order to obtain a clean, O and C free starting surface. Ge_2H_6 (1% diluted in H_2) and $SnCl_4$ (supplied by H_2 bubbling) were used as precursor gases. Sn contents and DSR were estimated from X-ray diffraction two dimensional reciprocal space map (XRD-2DRSM) results.

Figure 1 shows X-ray diffraction (XRD) measurement together with the modeling for a 25 nm-thick $Ge_{0.93}Sn_{0.07}$ layer. The XRD measurement reveals a pseudomorphic growth of the $Ge_{0.93}Sn_{0.07}$ layer on top of Ge buffer layer. Comparing with the modeling of the layers on a Ge substrate, we obtain a good correlation, showing a high crystallographic quality of the $Ge_{1-x}Sn_x$/Ge heterostructure. Bright photoluminescence (PL) also confirms the good material quality in terms of low defectivity [14].
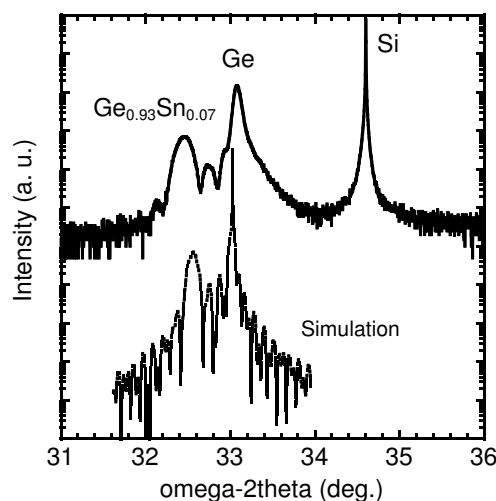

Figure 1. Measured (solid line) and simulated (dotted line) XRD (004) ω-2θ scan of a strained QW containing a 25 nm $Ge_{0.93}Sn_{0.07}$ layer embedded within a virtual Ge substrate and a 100 nm Ge cap layer.

Results and discussion

Ge$_{1-x}$Sn$_x$ QW photodetectors

Single QW Ge$_{1-x}$Sn$_x$ photodetector. In order to investigate the dependence of the QW photodetector responsivity on the Sn content, we fabricated single QW $Ge_{1-x}Sn_x$ photoconductors with various Sn contents [6]. 40 nm thick fully strained $Ge_{1-x}Sn_x$ layers, which have a Sn content of 0 (pure Ge), 5 and 9%, were grown on 0.5 µm thick Ge buffer layers grown on Si substrates. The $Ge_{1-x}Sn_x$ layers were capped with 50 nm thick pure Ge layers. Au/Ni comb electrodes were deposited on the $Ge_{1-x}Sn_x$ QW structure, and the photo responsivity was measured by the material conductivity change through the absorption of light with variable wavelength.
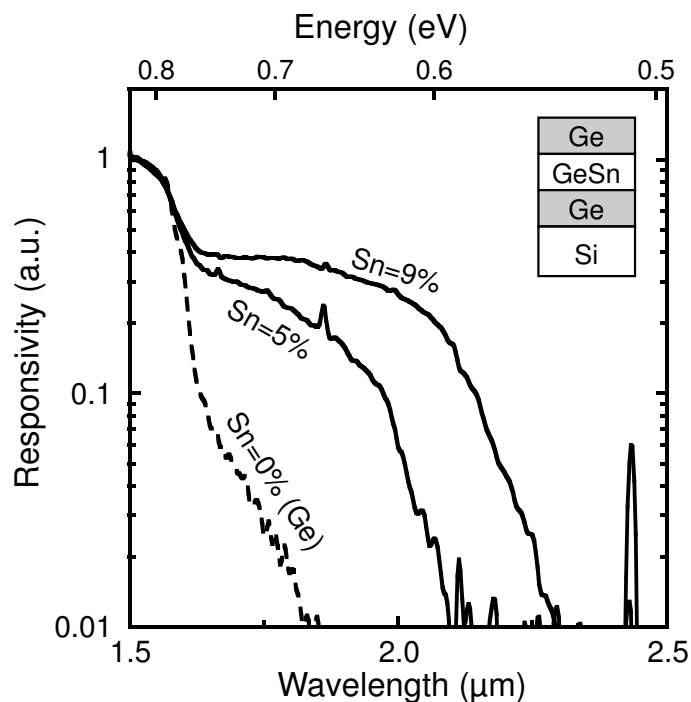
Figure 2. Normalized responsivity of single quantum well $Ge_{1-x}Sn_x$ photodetectors with different Sn content as a function of wavelength.

Figure 2 shows the photoconductor responsivity measured by photoconductivity measurement on the single QW $Ge_{1-x}Sn_x$ photodetectors with different Sn contents [6]. The detectable wavelength range is expanded with Sn introduction due to the band gap energy shrinkage. As a result, the responsivity increases with Sn content. The band gap values were estimated from the intersection with the zero absorption in linear plotting of the responsivity spectrum. The values are 0.63 eV and 0.57 eV for fully strained $Ge_{1-x}Sn_x$ layers with Sn content of 5% and 9%, respectively. These values are smaller than the values predicted by our theoretical calculations [5]. The reason for this discrepancy can be understood as follows. The 0.5 µm Ge buffer layer has tensile strain of 0.17% introduced by the thermal expansion mismatch between Ge and Si. Therefore, the coherently grown $Ge_{1-x}Sn_x$ layer on top of the tensily strained Ge buffer layer has a larger in-plane lattice constant than a pseudomorphic $Ge_{1-x}Sn_x$ layer grown on strain free Ge, which is assumed in the theoretical calculation. An increase of the in-plane lattice constant of the $Ge_{1-x}Sn_x$ layer makes the direct band gap smaller [5].

Multi-QW $Ge_{1-x}Sn_x$ photodetectors. As the photodetector responsivity is expected to increase with increasing $Ge_{1-x}Sn_x$ thickness, we assessed the impact of the total thickness of the absorption region on the responsivity by using multi-QW $Ge_{1-x}Sn_x$ layer structures. Multi QW structures enable to increase the thickness of the strained $Ge_{1-x}Sn_x$ adsorbing layer while preventing the unwanted formation of misfit dislocations [15]. Again, the QW structures were grown on 0.5 µm thick Ge buffered Si substrates. Each QW consists of a 20 nm thick fully strained $Ge_{1-x}Sn_x$ layer with a Sn content of 10% and a 100 nm thick Ge barrier layer. The total $Ge_{1-x}Sn_x$ thickness was increased by increasing the number of QWs (from 0 to 3).

Figure 3 shows the responsivity measured by photoconductivity measurement on the multi-QW $Ge_{1-x}Sn_x$ photodetectors with different number of QWs [6]. A higher responsivity is observed for the structure with a higher number of QWs. The detectors cut off at 2.4 µm. The actual responsivities measured by surface illumination with several light sources for the 3 QW photodetector are 2, 1, 0.3 and 0.1 A/W at 0.75, 1.5, 1.75 and 2.2 µm, respectively. In comparison with the 0 QWs photodetector, the 3 QWs photodetector has an approximately 2 times higher actual responsivity at 1.5 µm.
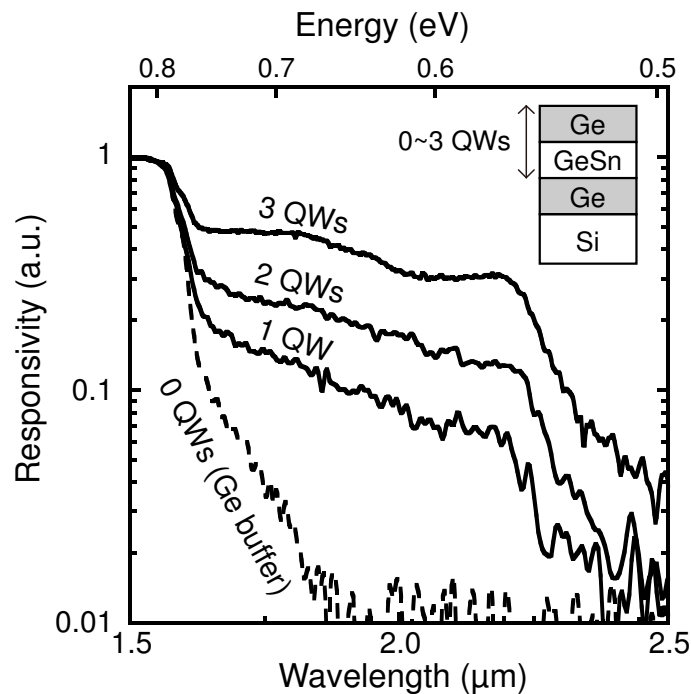

Figure 3. Normalized responsivity of multi-QW $Ge_{1-x}Sn_x$ photodetectors with Sn content of 10% and a different number of QWs as a function of wavelength.

Sn Surface agglomeration

Another option to increase the photodetector responsivity is by using a direct band gap material as an active region. A relaxed $Ge_{1-x}Sn_x$ layer with a sufficiently high Sn content is predicted to become a direct band gap material [5]. However, Sn surface agglomeration needs to be suppressed during the growth of thick relaxed $Ge_{1-x}Sn_x$ layers. As mentioned above, Sn surface agglomeration is the result of the collision among Sn atoms on the growing surface. To suppress it, the Sn surface atoms need to be frozen during the epitaxial $Ge_{1-x}Sn_x$ growth. It is expected that Sn surface migration can be reduced by using a higher growth rate and/or by using surfactant atoms. In addition, it is expected that the choice of the carrier gas (N_2 versus H_2) affects both Sn segregation toward the surface as well as the surface Sn migration because of the surfactant effect of hydrogen [16] and the surface H-termination, respectively.

$Ge_{1-x}Sn_x$ layers with a nominal Sn content of 10% were grown on 100 mm Ge substrates. The target thickness of the $Ge_{1-x}Sn_x$ layers is 200 nm. N_2 and H_2 were used as carrier gases with flows ranging from 10 to 40 slm. The used carrier gas flow and precursor partial

pressures (PPs) for each samples are summarized with measured growth rate, Sn content and DSR in Table I.

TABLE I. Growth conditions used to assess Sn surface agglomeration during epitaxial $Ge_{1-x}Sn_x$ growth by CVD.

Sample name	Carrier gas Flow (slm)	Ge_2H_6 PP (Pa)	$SnCl_4$ PP (Pa)	Measured Growth Rate (nm/min)	Measured Sn content (%)	Measured DSR (%)
20N-1	20 (N_2)	24.7	4.0	31.5	9.6	17
10N-2	10 (N_2)	91.6	11.1	33.0	10.7	50
20N-2	20 (N_2)	48.1	5.8	37.7	11.2	20
40N-2	40 (N_2)	24.7	3.0	32.2	6.8 and 1.5	-
10H-2	10 (H_2)	91.6	11.1	48.3	9.1	4
20H-2	20 (H_2)	48.1	5.8	43.2	9.1	63
40H-2	40 (H_2)	24.7	3.0	37.0	8.0	2

Figure 4 shows the $Ge_{1-x}Sn_x$ surface grown with different precursor flows in N_2 ambient (sample 20N-1 and 20N-2). The N_2 gas flow was 20 slm for both. As indicated by the arrows, the surface of the sample grown at a lower growth rate (Fig. 4a) has small and large white regions, which are the footprint of the Sn surface agglomeration. On the other hand, the sample grown at a higher growth rate (Fig. 4b) has a smooth surface except for a large white region at the center. This large white region appears only a limited region and might be caused by inefficient drying which was done manually after the wet HF treatment. Microscope inspections revealed that the shiny part on the wafers has a smooth surface without Sn agglomerations. This result indicates that the higher precursor PPs, which result in a higher growth rate, can suppress the Sn surface agglomeration by freezing Sn atoms into the subsurface.
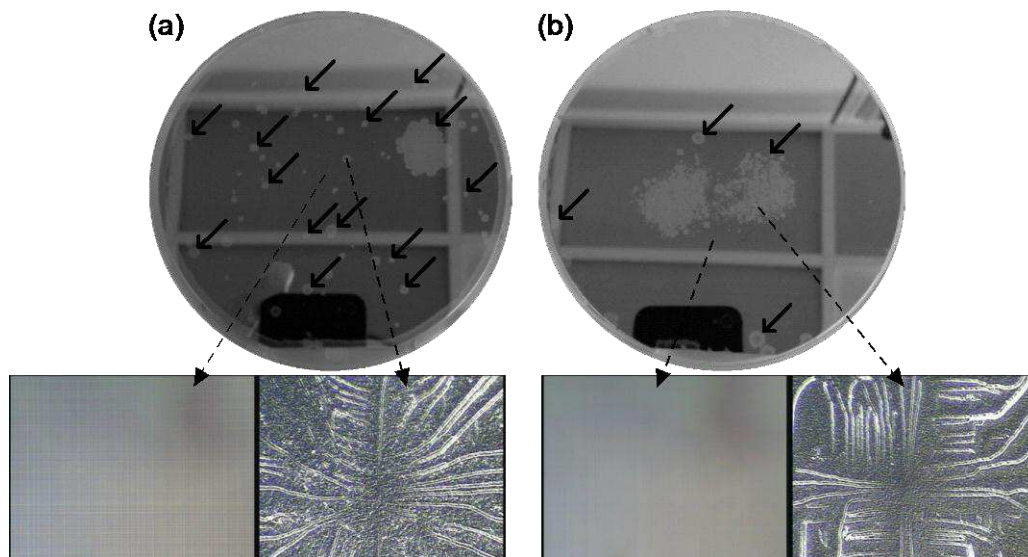

Figure 4. Surface of $Ge_{1-x}Sn_x$ layers grown in N_2 ambient with (a) low precursor PP (sample 20N-1) and (b) high precursor PP (sample 20N-2). The insets show microscope images taken on the shiny part and the white region on the surface as indicated by dotted arrows. Solid arrows indicate some of white regions. The reflection of the clean room ceiling and the camera (not related to the wafers) are also visible on the surface.

Figure 5 illustrates the impact of the N_2 carrier gas flow on the $Ge_{1-x}Sn_x$ surface quality (sample 10N-2, 20N-2 and 40N-2). Firstly, 20N-1 (Fig. 4a) and 40N-2 (Fig. 5c) obviously have a different surface morphology, although they were grown with the same Ge_2H_6 PP and at very similar growth rates. The very weak XRD peak (not shown) and the microscope inspection revealed that the surface of 40N-2 is polycrystalline. In addition, Sn precipitation occurred in the 40N-2 sample because two peaks corresponding to the $Ge_{1-x}Sn_x$ layers with 6.8% and 1.5% were observed in the XRD-2DRSM measurement.

Second, the impact of the precursor PP changed by the N_2 carrier gas flow on the Sn surface agglomeration cannot be clearly seen. As mentioned above, the large white region on the 20N-2 (Fig. 4b and 5b) might be due to inefficient drying. The growth rates of 20N-2 is higher than that of 10N-2 (37.7 and 33.0 nm/min, respectively), although the precursor PP is lower for 20N-2.

If N_2 is used carrier gas, gas turbulence might occur, due to the high density and the low thermal conductivity of N_2. In the higher N_2 flow case, the turbulence flow easily occurs (p.98 in Ref. 17), and which results to these non-predictable results. The gas turbulence complicates process control especially for such a sensitive $Ge_{1-x}Sn_x$ growth process.
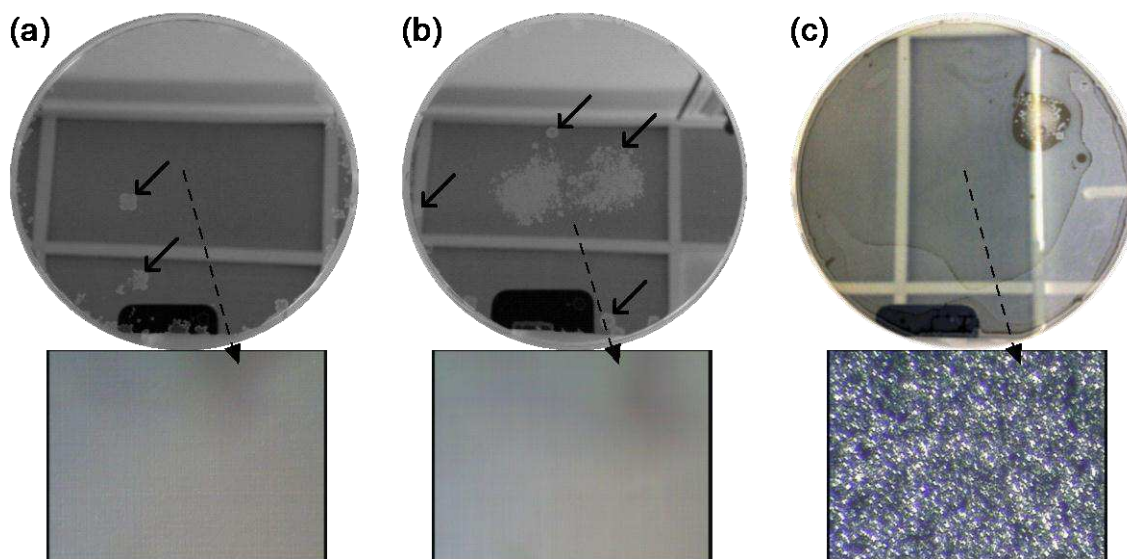

Figure 5. $Ge_{1-x}Sn_x$ surface for epitaxial layers grown in N_2 environment (a) 10 slm N_2 (10N-2), (b) 20 slm N_2 (20N-2) and (c) 40 slm N_2 (40N-2).

Figure 6 shows the $Ge_{1-x}Sn_x$ surface for different H_2 carrier gas flows (sample 10H-2, 20H-2 and 40H-2). The growth rate increases with decreasing H_2 flow (Table I). This indicates that no turbulence happens if the $Ge_{1-x}Sn_x$ proceeds in H_2.

The lower H_2 flow case has a high density of small white spots caused by Sn agglomeration, despite of the higher growth rate (sample 10H-2, Fig. 6a). This result is repeatable. In addition, a large white region corresponding to polycrystalline material is observed on the surface. We believe that this is caused by a too high supply of precursors

resulting in this epitaxial breakdown with Sn agglomerations as observed by the microscope inspection.

Before we discuss the observations as seen for the samples grown at higher H_2 flows (Fig. 6b and 6c), we will first briefly introduce the velocity boundary layer thickness and its variation as function of the different growth conditions (p. 137 in Ref. 17). The velocity boundary layer is defined as the layer between the substrate surface and the constant gas flow region in the reactor. The velocity of the gases is constant at the region far from the substrate/susceptor. However, it is well known that it is reduced near the substrate/susceptor. The velocity boundary layer thickness, $\delta(x)$, is given as [17]:

$$\delta(x) = 4.64 \, (\mu x \, / \, \rho U_0)^{0.5} \tag{1}$$

where, μ denotes the viscosity coefficient of the carrier gas, x denotes the position from the edge of susceptor along the gas flow, and ρ denotes the density of the carrier gas. U_0 denotes the gas velocity in the constant gas flow region and is mainly defined by the carrier gas flow. The precursor gases diffuse toward the substrate from the constant gas flow region over the substrate via the velocity boundary layer. The velocity boundary thickness is helpful to consider the supply of precursor gases toward the substrate in different carrier gas conditions.

The increase in carrier gas flow might affect the growth characteristics in several ways. First, the higher gas flow leads to an increase in gas velocity and a reduction in the thickness of the velocity boundary layer. This is expected to result in a faster supply of both the Ge and Sn precursor gases (or of their reactants) to the growing surface. Second, a higher carrier gas flow, reduces the PPs of the both the Ge and Sn precursors. Both of them might affect the Sn incorporation in the layer. Experimentally, we observed that for H_2 as carrier gas, an increase in carrier gas flow results in a reduced Sn incorporation in the epitaxial layer (Table I).

Because of the lower density of H_2 the velocity boundary layer is thicker for H_2 compared to N_2. Nevertheless, the $Ge_{1-x}Sn_x$ growth rate is higher if H_2 is used as a carrier gas. For the chosen process conditions, the $Ge_{1-x}Sn_x$ growth proceeds in the mass-transfer regime. The observed increase in growth rate using H_2 as carrier gas therefore indicates that higher amounts of precursor gases reach the growing surface. This is explained by their higher gas diffusion coefficient in H_2. In addition, the H-termination of the growing surface is expected to be higher in H_2 environment. Experimentally, we observed a reduction in Sn incorporation if N_2 as carrier gas is replaced by H_2.

Because of the higher growth rate and the surfactant effect of H [16], Sn surface agglomeration is expected to be lower if $Ge_{1-x}Sn_x$ growth proceeds in H_2 environment. However, we observed a higher degree of Sn agglomerations on the surface for layers grown with 20 slm H_2 (Fig. 6b) than those grown with 20 slm N_2 (Fig. 5b). There is a need for a better fundamental understanding of the detailed reaction mechanism of the epitaxial growth process as well as of the impact of the carrier gas on this reaction mechanism. In addition, the behavior of the precursor gases during the diffusion through the velocity boundary layer and the impact of cleaning/drying efficiency on the Sn surface agglomeration needs a better understanding.

A higher H_2 flow of 40 slm results in a suppression of the Sn surface agglomeration (sample 40H-2, Fig. 6c). This result can be understood in terms of the H surfactant effect. The growth temperature (320°C) is close to the temperature at which adsorbed H starts to thermally desorb from the Ge surface (340°C) [16,18]. However, the H desorption can be suppressed by a higher H_2 supply. With increasing H_2 flow, the velocity boundary layer thickness reduces. The thinner velocity boundary layer enables a higher H_2 supply to the growing surface, although the H_2 PP is hardly affected. The Sn segregation should be suppressed by the surfactant effect of surface H [16]. As our intention is to use *relax* $Ge_{1-x}Sn_x$ as direct band gap material in optical devices, we measured the DSR using XRD-2DRSM. For sample, 40H-2, which contains 8% substitutional Sn, we measured a DSR of only 2% despite of the thickness which is 240 nm which is far above the critical thickness for layer relaxation. A post deposition annealing is needed to increase the strain relaxation. For these layers, Sn agglomeration during post deposition anneal still needs to be studied.
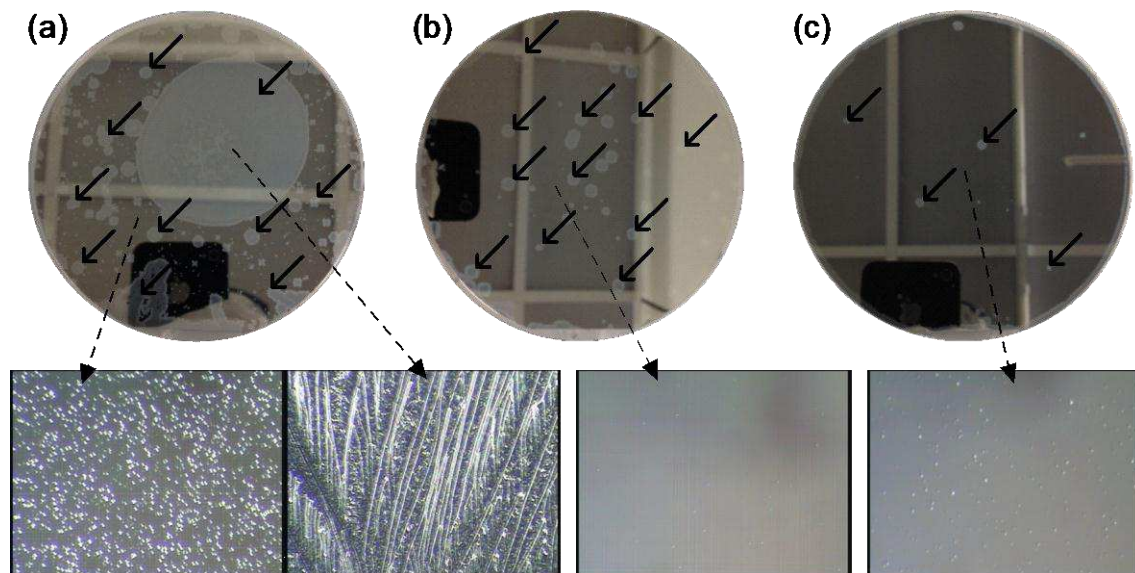

Figure 6. $Ge_{1-x}Sn_x$ surface for epitaxial layers grown in H_2 environment (a) 10 slm H_2 (10H-2), (b) 20 slm H_2 (20H-2) and (c) 40 slm H_2 (40H-2).

Conclusion

$Ge_{1-x}Sn_x$ has been considered as a promising candidate for both electrical and optical devices. Previously, nMOS devices with a promising effective electron mobility have been demonstrated. In this paper, we focused on optical devices and demonstrated the increase of the responsivity with increasing Sn content in fully strained $Ge_{1-x}Sn_x$ photodetectors. This is due to the shrinkage of the $Ge_{1-x}Sn_x$ band gap. The smaller band gap values compared to pure Ge for these $Ge_{1-x}Sn_x$ layers were estimated from the responsivity spectrum. A further enhancement of the responsivity was achieved by increasing the total thickness of the absorbing region, using a multi QW structure to avoid strain relaxation which would result in the introduction of unwanted dislocations.

Another option to enhance the efficiency of photodetectors is using a direct band gap material such as strain relaxed $Ge_{1-x}Sn_x$ with a sufficiently high Sn content (>11%) as an active layer. The issue to be addressed is the Sn surface agglomeration which relates to the

Sn surface segregation. The Sn surface agglomeration happens when the layer thickness is increased to achieve high DSR and a low threading dislocation density. We focused on freezing Sn atoms into the subsurface during $Ge_{1-x}Sn_x$ layer growth by increasing the growth rate which is experimentally done by changing the precursor PP. We found that higher precursor PPs, enhanced by using higher precursor flows, enable to suppress the Sn surface agglomeration. In addition, we investigated the impact of the chosen carrier gas and its flow on Sn agglomeration. If N_2 is used as a carrier gas, it is difficult to control the Sn agglomeration by increasing the gas flow because of its gas properties as there is a high risk for gas turbulence in the reactor. On the other hand, if H_2 is used as a carrier gas, a higher H_2 flow suppresses the Sn surface agglomeration. This can be explained by the surfactant effect of H.

Photodetectors based on strained $Ge_{1-x}Sn_x$ / Ge multi QW structures show promising results. But to realize photodetectors based on direct band gap materials using relaxed $Ge_{1-x}Sn_x$, there are still some challenges to be addressed. In particular, the layer quality has to be improved. We have reported, especially for thick $Ge_{1-x}Sn_x$ layers, the presence of corn shaped amorphous regions on the layer surface [9]. These amorphous regions degrade the quality of both electrical and optical devices and also might be a nucleation point for Sn agglomerations. However, its origin and the solution to avoid the amorphous corn have not been unambiguously clarified yet. Moreover, the complete prevention of Sn surface agglomeration is still to be achieved. In terms of the optical device design, the strained $Ge_{1-x}Sn_x$ multi QWs photodetector has the benefit that they can be grown with less dislocations. On the other hand, the strain relaxed direct band gap $Ge_{1-x}Sn_x$ photodetector can use a high efficient direct transition material. We have to clarify the impact of dislocations and direct band transition on the photodetector responsivity to achieve higher efficiency.

Acknowledgments

References

1. S. Gupta, *et al.*, *ECS Trans.* **50**(9), 937 (2012).
2. G. Han, *et al.*, *IEDM Tech. Dig.* 402 (2011).
3. R. Loo, *et al.*, *ECS J. Solid State Science and Technol.* **2**(1), N35 (2013).
4. M. V. Fischetti and S. E. Laux, *J. Appl. Phys.* **80**(4), 2234 (1996).
5. Y. Shimura, *et al.*, *8th International Conference on Si Epitaxy and Heterostructures (ICSI-8), abstract*, 65 (2013).
6. A. Gassenq, *et al.*, *Opt. Express*, **20**(25), 27297 (2012).
7. D. W. Jenkins and J. D. Dow, *Phys. Rev. B*, **36**, 7994 (1987).
8. Y. Shimura, *et al.*, *Thin Solid Films*, **518**, S2 (2010).

9. F. Gencarelli, *et al.*, *ECS J. Solid State Science and Technol*. **2**(4), P134 (2013).
10. G. Grzybowski, *et al*., *Appl. Phys. Lett.* **101**, 072105 (2012).
11. S. Wirths, *et al.*, *ECS J. Solid state Science and Technol*. **2**(5), N99 (2013).
12. G. Wang, *et al.*, *Appl. Phys. Lett.* **94**, 102115 (2009).
13. E. Kasper, *et al.*, *Thin Solid Films*, **520**, 3195 (2012).
14. S. Gupta, *et al.*, *proc. IEDM*, 16.2 (2012).
15. Y. Shimura, *et al.*, *Materials for Advanced Metallization 2013 (MAM2013) abstract book*, 239.
16. A. Sakai and T. Tatsumi, *Appl. Phys. Lett.* **64**, 52 (1994).
17. R. B. Bird, *et al.*, *Transport Phenomena: 2nd Edition*, Wiley, New York (2002).
18. L. Surnev and M. Tikhov, *Surf. Sci.* **138**, 40 (1984).